Experimental and atomistic modeling study of ion irradiation damage in thin crystals of the TiO_2 polymorphs

Gregory R. Lumpkin,* Katherine L. Smith, Mark G. Blackford, Bronwyn S. Thomas, and Karl R. Whittle
Institute of Materials and Engineering Science, Australian Nuclear Science and Technology Organisation, Private Mail Bag 1, Menai, NSW 2234, Australia

Nigel A. Marks
School of Physics, The University of Sydney, Sydney, NSW 2006, Australia

Nestor J. Zaluzec
Materials Science Division, Argonne National Laboratory, 9700 South Cass Avenue, Argonne, Illinois 60439, USA
(Received 10 October 2007; revised manuscript received 24 April 2008; published 13 June 2008)

Thin crystals of rutile, brookite, and anatase were irradiated *in situ* in the intermediate voltage electron microscope (IVEM-Tandem Facility) at Argonne National Laboratory using 1.0 MeV Kr ions at a temperature of 50 K. Determination of the critical amorphization fluence has revealed a large difference in the radiation tolerance. Synthetic rutile remained crystalline up to a fluence of 5×10^{15} ions cm^{-2} and did not show convincing evidence for the onset of amorphization at this fluence level. Natural brookite and anatase, on the other hand, became amorphous at $8.1\pm1.8\times10^{14}$ and $2.3\pm0.2\times10^{14}$ ions cm^{-2}, respectively. These results correlate with the number of shared edges, the degree of octahedral distortion, and the volume properties of polymorphs, and we show that the distortion and the volume are intimately linked through interatomic forces in the octahedral framework. The static and dynamic defect calculations indicate that the radiation tolerance of rutile is related, at least in part, to low energy migration pathways for both O and Ti. In order to gain further insight into the problem, we performed molecular dynamics (MD) simulations of small thermal spikes for each polymorph. These simulations are in qualitative agreement with the experiments, with the thermal spikes showing the same relative recovery behavior between the rutile, the brookite, and the anatase structures. The examination of previous MD simulations of TiO_2 glasses and experimental work on synthetic TiO_2 materials produced at low temperature provides a conceptual model for the structure of amorphous TiO_2 produced by ion irradiation of the crystalline polymorphs.

DOI: 10.1103/PhysRevB.77.214201 PACS number(s): 61.80.Jh, 61.82.Ms, 31.15.xv

I. INTRODUCTION

TiO_2 compounds have a number of important industrial and technological applications, including its use in pigments, photocatalysis, oxygen sensors, and thin film devices (e.g., antireflective coatings, waveguides, and optical amplifiers).[1] TiO_2 is also an important chemical component of polyphase and single-phase ceramic nuclear waste forms.[2] There are three common polymorphs of TiO_2: rutile, anatase, and brookite. Two less common high-pressure polymorphs have been found in nature. One of these, TiO_2 II, has the alpha-PbO_2 structure and occurs in terrestrial rocks, while a form with the baddeleyite structure has been found in a meteorite sample.[3] These and other high-pressure forms have been reported from laboratory syntheses and the general sequence of structure types with increasing pressure appears to be rutile $\rightarrow TiO_2$II $\rightarrow$ baddeleyite $\rightarrow$ orthorhombic phases (fluorite and cotunnite structures).[4–6]

To date, most ion irradiation studies of TiO_2 compounds have been conducted on rutile. Changes in the electrical properties, the site location of implanted ions, and the transport phenomena of single crystal rutile specimens irradiated with a range of metal ions have been reported extensively by Fromknecht and co-workers.[7–13] These authors have also investigated the damage recovery of ion-implanted rutile and we will address these results later in the discussion. In other studies, rutile has been reported to be susceptible to amorphization upon bombardment with 360 keV Xe ions at room temperature.[14–16] Sickafus *et al.*[16] have commented that the observed amorphization of rutile is in contrast with the general radiation resistance of a range of A_2O_3 and BO_2 compounds, and they imply that the structure type is a major factor controlling the radiation tolerance of these simple oxides as long as the formal ionic radii of the cations are similar.

In this work, we test the structure type criterion and other potential factors affecting the susceptibility to amorphization using samples of the low-pressure TiO_2 polymorphs rutile, brookite, and anatase. A particular advantage of this choice of materials is that the structural aspects can be evaluated in the absence of any major differences in the chemical composition. Additionally, the degree of covalence is similar between the three compounds and the bonding is described by molecular orbital formation involving interactions between the Ti $3d$, $3s$, and $3p$, with the O $2p$ and $2s$ atomic orbitals.[17] Spectroscopic studies consistently reveal splittings of around 3 eV between the unoccupied t_{2g} and e_g energy levels in the Ti $L_{2,3}$ and O K absorption edges (additional splittings of the e_g band may be observed depending on the Ti site symmetry).[18,19] Furthermore, the theoretical analysis of

rutile, brookite, and anatase has shown that all three phases can be well described by a fixed partial charge model,[20] akin to prescribing a fixed covalency. The high level of agreement between the atomistic model and the experiment provides strong evidence that any variation in covalency among these polymorphs is small, if not negligible.

In this paper, we focus on the relationships between the polyhedral distortion and the volume elements of TiO_2 polymorphs, and illustrate the correlations of susceptibility to ion irradiation damage. Specific results of this paper are discussed in light of previous experimental works on amorphous TiO_2, MD simulations of fully dense TiO_2 glass, and previous spectroscopic work on the local structure and bonding of amorphous TiO_2 produced by ion irradiation of rutile single crystals. We provide additional static defect calculations together with MD simulations of small collision cascades (thermal spikes) in order to explore the mechanisms of radiation damage and recovery in greater detail.

II. SAMPLES AND METHODS

The rutile sample used in this study consisted of a fragment of a pale yellow single crystal grown via the lead pyrophosphate flux method. In order to examine the effect of crystalline structure on the radiation response, we used natural samples of anatase (G24530, Matshorhae, Ullensvang, Norway) and brookite (G17291, Fron-oleu, Tremadoc, Caernarfonshire, Wales). Electron beam microanalyses of the synthetic and natural TiO_2 polymorphs were obtained from polished sections of the samples using a JEOL JSM-6400 scanning electron microscope operated at 15 kV and equipped with a Noran Voyager energy dispersive spectrometer. The instrument was operated in standardless mode; however, the sensitivity factors were calibrated for semiquantitative analysis using a range of synthetic and natural standard materials. The spectra were usually acquired for 500 s, reduced to weight percent oxides using a digital top hat filter to suppress the background and a library of reference spectra for multiple least-squares peak fitting. Results show that the rutile, brookite, and anatase samples have purity levels of 99.9, 99.5, and 99.6 wt % TiO_2, respectively. The main impurities detected in the samples are Nb, Si, Al, V, Cr, and Fe. Selected crystal structure data, distortion, and volume parameters of the polymorphs are summarized in Table I. Equations used in the calculation of polyhedral volume and distortion parameters are described in Appendix A.

Transmission electron microscope (TEM) samples were prepared by crushing small fragments in methanol and collecting the suspension on holey carbon coated copper grids. All specimens were plasma cleaned to minimize contamination. Ion irradiation experiments were carried out *in situ* at the IVEM-Tandem User Facility at Argonne National Laboratory with 1.0 MeV Kr ions using a Hitachi TEM interfaced to a NEC ion accelerator.[21] All TEM observations were carried out using an operating voltage of 300 kV; however, the electron beam was always turned off during the irradiation steps in order to avoid unnecessary complications arising from the simultaneous ion–electron interactions. The ion irradiations were performed using a flux of 6.25 $\times 10^{11}$ ions cm^{-2} s^{-1} and were conducted with the *x*-axis and *y*-axis tilt drives of the TEM set at 0° and 13°, respectively (the sample was tilted toward the ion beam in order to prevent shadowing and reduced ion counts).

TABLE I. Summary of structural, polyhedral distortion, and volume data for the TiO_2 polymorphs.

	Rutile	Brookite	Anatase
Space Group	$P4_2/mnm$	$Pbca$	$I4_1/amd$
Z	2	8	4
Shared edges	2	3	4
a cell edge (Å)	4.594	9.174	3.784
b cell edge (Å)	4.594	5.449	3.784
c cell edge (Å)	2.959	5.138	9.515
Cell volume ($Å^3$)	62.45	256.84	136.24
Molar volume (cm^3 mol^{-1})	18.80	19.33	20.51
Density (g cm^{-3})	4.248	4.132	3.895
Packing Index	70.46	68.53	64.59
Octahedral Volume ($Å^3$)	9.903	9.761	9.473
Octahedral Volume ($Å^3$) θ=90°	10.02	10.03	9.871
$(Ti\text{-}O)_{ave}$ (Å)	1.959	1.960	1.949
Bond Length Distortion ($\Delta_{Ti\text{-}o}$)	0.790	2.754	1.063
Edge Length Distortion ($\Delta_{o\text{-}o}$)	3.097	4.752	6.912
Bond Angle Variance (σ_θ^2)	28.67	65.23	105.15
Quadratic Elongation ($\langle\lambda\rangle_{oct}$)	1.008	1.019	1.028

Experiments were performed at a temperature of 50 K using a sample holder equipped for liquid He cooling. To avoid the potential effects of ion channeling, the grains were irradiated in random orientations. Each sample was irradiated using incremental fluence steps, and the selected grains were observed using bright field imaging and selected area diffraction after each irradiation step. Using photographic negatives or digital images, the critical amorphization fluence (F_c) was constrained to fall between the last dose increment, in which Bragg diffraction spots were observed, and the next increment, in which only diffuse rings occur in the diffraction pattern. For each sample, we determined F_c from the average of several different grains.

The reliability of the experimental procedure was checked using a high quality specimen of Nd doped zirconolite 2M. This sample returned a critical fluence of $4.1 \pm 0.2 \times 10^{14}$ ions cm^{-2} and is within error of the previous determinations that we have made on a yearly basis since 1998. Note that in the submission process, a reviewer criticized our experimental procedures, claiming that the grains are prone to adverse heating in the ion beam due to poor contact with the carbon film. In answer to this, we provide a detailed summary of previous measurements using both crushed grains and ion beam thinned (IBT) samples in Appendix B. Additional comments on the heat flow problem are addressed in Appendix C. The experimental data and calculations clearly illustrate that both experimental methods produce essentially the same results.

Static calculations of the O and Ti Frenkel defect formation energies for all three polymorphs were carried out

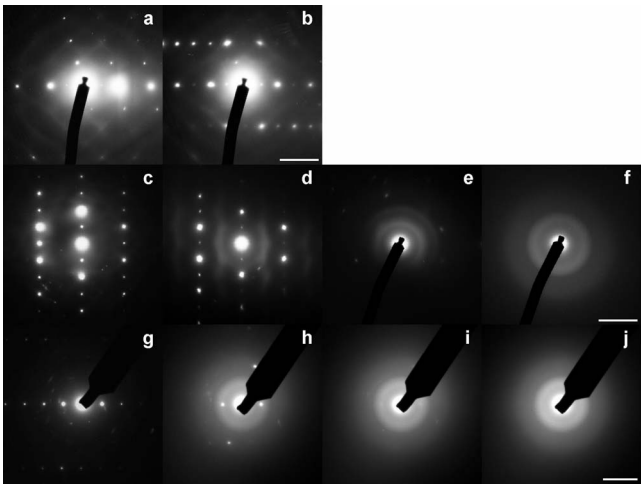

FIG. 1. SAED patterns of TiO_2 polymorphs irradiated with 1.0 MeV Kr ions at 50 K. Top row: Rutile close to [012] zone, (a) unirradiated and (b) after a fluence of 5×10^{15} ions cm^{-2}. Second row: Brookite [011] zone, (c) unirradiated and after fluences of (d) 3.1×10^{14}, (e) 6.3×10^{14}, and (f) 1.5×10^{15} ions cm^{-2}. Bottom row: Anatase (011) systematic row, (g) unirradiated and after (h) 1.3×10^{14} ions cm^{-2}, (i) 1.9×10^{14} ions cm^{-2}, and (j) 2.8×10^{14} ions cm^{-2}. Scale bars at the end of each row are equivalent to ~0.26 $Å^{-1}$ in reciprocal space.

within the program GULP[22] using the Mott–Littleton[23] method. The Frenkel defect energies that were calculated using this approach represent the sum of the energies of the isolated interstitial and isolated vacancy. In order to gain further insight into the recovery of damage on picosecond time scales, we performed MD simulations of small thermal spikes using the DL_POLY package.[24] We considered thermal spikes typically containing 130 atoms as prototypical systems for ion irradiation damage in thin crystals. The thermal spike was embedded in a large crystalline matrix using near-cubic supercells of around 5000 atoms. The atoms in a central sphere of radius 7 Å were given an initial kinetic energy of 6 eV per atom with all other atoms initially at 0 K. All of the defect calculations and MD simulations reported in this paper employ the interatomic pair potential model of Matsui and Akaogi.[20]

III. EXPERIMENT DATA

The results of the irradiation experiments are summarized in Fig. 1 in the form of selected area electron diffraction (SAED) patterns recorded at various fluence steps during irradiation. The synthetic rutile clearly remained crystalline up to a fluence of 5×10^{15} ions cm^{-2} [Figs. 1(a) and 1(b)]. The rutile sample shows very little evidence of structural damage with increasing fluence and most importantly, the close inspection of the SAED pattern failed to show clear evidence of damage in the form of a weak diffuse ring. This observation indicates that there is no significant accumulation of amorphous domains in synthetic rutile at the maximum fluence of this study.

Brookite [Figs. 1(c)–1(f)] and anatase [Figs. 1(g)–1(j)], on the other hand, are both susceptible to amorphization under

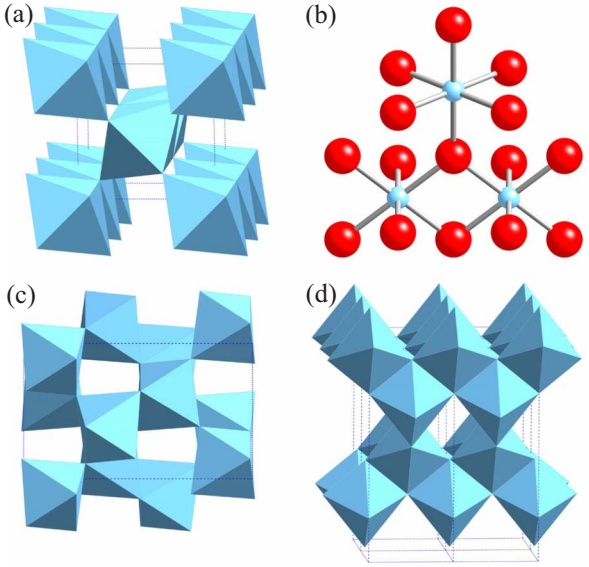

FIG. 2. (Color online) Crystal structures of the three common TiO_2 polymorphs: (a) Rutile, which have two shared edges per octahedron, forming linear chains connected by corner sharing. This view is tilted off [001]. Note the straight tunnels consisting of vacant octahedral sites. (b) A ball and stick model of part of the rutile structure illustrating the nature of the edge and corner shared linkages. (c) Brookite, which have three shared edges per octahedron, forming zigzag chains connected by corner sharing. This is viewed down [001]. The open space is due to the presence of zigzag chains of vacant octahedral sites in this direction. (d) Anatase, which have four shared edges per octahedron, forming a complete three-dimensional framework. This view is tilted off [100]. Note the presence of tunnels in this direction. More complex tunnels also exist along the ⟨111⟩ directions.

the conditions of these experiments and returned F_c values of $8.1\pm1.8\times10^{14}$ and $2.3\pm0.2\times10^{14}$ ions cm^{-2}, respectively. The progression of damage in these two polymorphs is typical of many oxide compounds that pass through the crystalline–amorphous transformation. In the very early stages of damage, only sharp Bragg diffraction spots are observed while in the next stage, the intensities of these spots begin to diminish and this generally coincides with the first appearance of diffuse rings in the SAED patterns. Ultimately, the Bragg spots disappear altogether, an indication that the amorphous state has been reached.

The real space peak positions of the strongest diffuse correlation rings in the SAED pattern of brookite were found to be approximately 0.18 and 0.31 nm. Values of about 0.17 and 0.31 nm were found for anatase, suggesting that the amorphous structures derived from the two polymorphs are broadly similar; however, the confirmation of this awaits detailed analysis of the radial distribution functions together with spectroscopic studies of the local coordination and bonding. The measured real space peak positions are also similar to those of other oxide compounds containing Ti and other elements (e.g., Nb and Ta) in octahedral coordination, and are related to the pair correlations representing the first and second coordination spheres, respectively.[25,26]

IV. DISCUSSION

A. General comments

As noted in the Introduction, rutile has been studied extensively via implantation of ions with different oxidation states, while anatase and brookite less so. For rutile single crystals irradiated with 300 keV La ions at temperatures of 77 and 300 K, complete amorphization is observed at fluences of 1×10^{15} and 2×10^{15} ions cm^{-2}, respectively.[7] Other results, summarized for a range of ions (e.g., Sb, Au, Hg, Sn, In, Pb, etc.) implanted into the rutile single crystals at relatively low energies (typically 150–300 keV),[11] reveal that there are three recovery stages at 77, 170–210, and 260–293 K. These results illustrate that rutile can be rendered amorphous but under very different conditions to the experiments conducted in this paper. Calculations using the SRIM 2003 (The Stopping and Range of Ions in Matter) (Ref. 27) indicate that, for 300 keV La ions implanted into bulk rutile, the electronic to nuclear stopping power ratio is 0.10 and only 6.7% of the energy loss is due to ionization by the La ions. This compares to a value of ENSP=0.79 for 1.0 MeV Kr ions, which lose 48%–56% of their energy by ionization when transmitted through the rutile crystals with thicknesses of 50–100 nm.

Previous results[14,15] also indicate that the single crystals of rutile can be amorphized upon irradiation with 360 keV Xe, with the reported critical fluence values of 4×10^{14} ions cm^{-2} at a temperature of 160 K and 8×10^{15} ions cm^{-2} at 300 K. It was also reported that TEM specimens of rutile become amorphous during *in situ* experiments with 1.5 MeV Xe ions with a critical amorphization temperature of 200 K. Experiments were also conducted on rutile using 1.5 MeV Kr ions with amorphization reported at temperatures of 15–130 K and critical fluence values of approximately 8×10^{14} to 3.5×10^{15} ions cm^{-2}.[14] These results are at a variance with our experiment on high-purity synthetic rutile, which did not become amorphous up to a fluence of 5×10^{15} ions cm^{-2} when irradiated with 1.0 MeV Kr ions at 50 K. A possible explanation for this discrepancy involves the chemical purity of the rutile sample used in Ref. 14. In work to be reported elsewhere, we have irradiated rutile crystals with 1.0–2.0 wt % impurities, finding that F_c is approximately 10^{15} ions cm^{-2} at 50 K (e.g., similar to that of brookite).

B. Polyhedral distortion

The critical fluence data reported in this paper correlate inversely with the number of shared edges per TiO_6 octahedron in each structure: two for rutile, three for brookite, and four for anatase. The crystal structures and the nature of the octahedral frameworks of these polymorphs are shown in Fig. 2 where we can see the relatively simple tetragonal structure of rutile with chains of edge sharing octahedra (site symmetry *mmm*) parallel to [001], connected by corner sharing [Fig. 2(a)]. Brookite, on the other hand, is orthorhombic and with three shared edges per octahedron (site symmetry 1) adopts a more complicated structural framework consisting of zigzag chains connected by edge and corner sharing [Fig. 2(c)]. With four shared edges per octahedron, the framework of anatase is more regular and the crystal system is tetragonal; however, the TiO_6 octahedron is significantly distorted in this polymorph and can be described more accurately as a scalenohedron with site symmetry $\bar{4}m2$ [Fig. 2(d)]. All of the structures being based upon a distorted closest packed array of anions contain vacant octahedral and tetrahedral sites nestled within the oxygen array. The most likely interstitial positions for Ti are the vacant octahedral sites or similar positions within the tunnels. It is unlikely that the tetrahedral sites are occupied by Ti interstitials due to the very short Ti-Ti distances (~1.7–1.9 Å) across shared octahedral faces, leading to destabilization due to strong electrostatic repulsion.

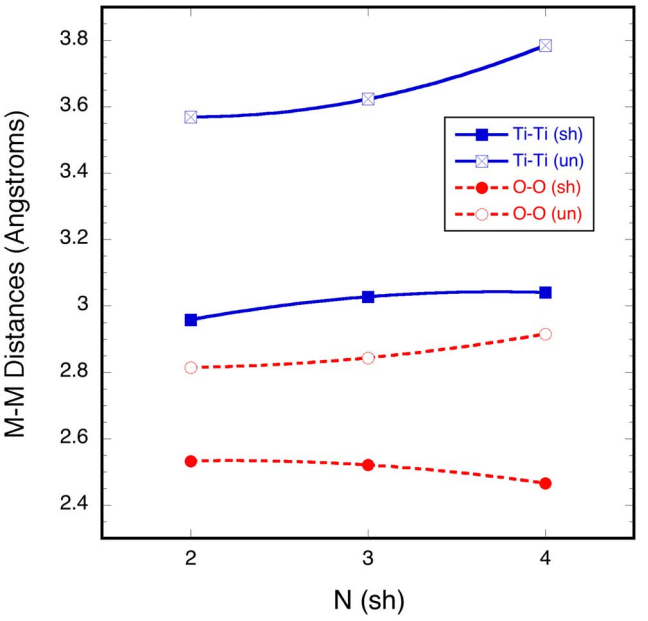

FIG. 3. (Color online) Plots of the mean shared and unshared Ti-Ti and O-O distances (Å) versus the number of shared edges for rutile (2 shared edges), brookite (3 shared edges), and anatase (4 shared edges). The O-O distances are shown as circles connected by dashed lines (red) and reflect changes in the electrostatic and short-range contributions to the interatomic potential. Note that the mean O-O separation is nearly the same in all three polymorphs. The Ti-Ti distances are shown as squares connected by solid lines (blue) and reflect, in part, the electrostatic repulsive forces across the shared edges. The framework Ti-Ti distances exert a strong influence on the volume of these octahedral structures. This is the origin of the relationship between distortion and volume discussed in the text.

A characteristic feature of edge sharing in the octahedral framework structures is an increase in the distortion of the coordination polyhedra as the shared edges become shorter and the unshared edges become longer [see Fig. 2(b)]. In classical terms, these distortions are viewed as the result of strong electrostatic cation–cation repulsions across the shared edges.[28] Changes in the metal–metal distances of the TiO_2 polymorphs are shown graphically in Fig. 3, where we see that the average shared O-O distance decreases and the average unshared O-O distances decrease with increasing number of shared edges. Thus, the TiO_6 octahedra of the three polymorphs become more distorted from rutile to broo-

kite to anatase. In order to quantify this effect, we calculated the bond length distortion ($\Delta_{Ti\text{-}O}$), edge length distortion ($\Delta_{O\text{-}O}$), octahedral angle variance (σ_θ^2), and quadratic elongation ($\langle\lambda\rangle_{oct}$) parameters using the equations given in Appendix A.[29,30] The data shown in Table I reveal that the edge length distortion, octahedral angle variance, and quadratic elongation parameters all increase systematically from rutile to brookite to anatase. The bond length distortion does not follow the same pattern and brookite is much more distorted in this respect than the other two polymorphs. This effect is related in part to the lower symmetry of brookite where, in the average structure, all six Ti-O bond lengths are unconstrained by symmetry and are free to adjust independently with respect to the interatomic forces.

At present, there are very few details on the structures and properties of the amorphous forms of TiO_2 produced by ion irradiation of the different polymorphs. However, the diffuse scattering distributions in the SAED patterns of irradiated brookite and anatase are nearly identical (Fig. 1), suggesting that the amorphous structures (e.g., pair correlation functions) are similar. Recent MD simulations of the amorphous structure of TiO_2 formed by rapid cooling from the liquid state indicate that the first coordination sphere (Ti-O) remains largely intact, with a mean Ti-O distance of approximately 1.77–1.85 Å and mean Ti coordination number of 5.4–5.8.[31,32] These values indicate a reduction in the average bond length and coordination number in the amorphous structure. However, the magnitude (about 0.1–0.2 Å) of the reduction in mean Ti-O bond lengths relative to the crystalline polymorphs under consideration here is quite large when compared with previous x-ray absorption spectroscopy (XAS) studies of Ti in radiation damaged complex oxides.[33] These low Ti-O distances in the simulated glasses must be reconciled against the experimental data (see Ref. 34 and further discussion below).

The Ti-Ti partial pair distributions returned by the MD simulations cited above range from about 2.8 to 3.9 Å with distinct peaks near 3.0 and 3.5 Å. These data indicate that simulated TiO_2 glass contains both edge shared (shorter) and corner shared (longer) linkages, giving Ti-Ti distances similar to the crystalline phases (e.g., 2.95–3.06 Å for edge sharing and 3.5–3.8 Å for corner sharing). Furthermore, the ratio of the two peaks in the reduced pair distribution function $G(r)$ is approximately 1:1.5 (see Fig. 1 in Hoang's paper[31]), indicating that the proportion of edge versus corner shared Ti-Ti distances in the amorphous TiO_2 glass falls between that of brookite (1:2) and anatase (1:1). For comparison, this ratio is 1:4 in rutile. The Ti-O-Ti bond angle distributions for the simulated TiO_2 glasses[31,32] have also been calculated and they show peaks near 105° and 130°, related to shorter Ti-Ti distances across shared edges and longer Ti-Ti distances across shared corners, respectively.

Amorphous TiO_2 has been produced and characterized by a number of different methods at low temperature. Petkov *et al.*[34] studied the atomic scale structure of the material produced by sputtering and sol-gel methods using diffraction and reverse Monte Carlo simulations. For the first coordination sphere, these authors determined a mean Ti-O distance of 1.96 Å and coordination number of 5.4 ± 0.4, and, for the second coordination sphere, they found two Ti-Ti distances of about 3.0 and 3.6 Å. They concluded that the amorphous structure consisted of edge sharing TiO_6 chains with similarities to the structure of brookite. Other investigators have used XAS to study the amorphous TiO_2 produced via low temperature synthesis and find that the structures have similarities to the crystalline anatase.[35,36] Some details of the real amorphous structure produced by ballistic processes are provided by recent XAS measurements of rutile following irradiation with 340 keV Xe ions to a fluence of 1.5×10^{15} ions cm^{-2}. In this work, the experimental Ti $L_{2,3}$ spectra of the amorphous phase indicate that the local coordination and bonding are similar to anatase.[37]

C. Volume properties

As shown in Table I, the molar volume of the TiO_2 polymorphs increases from rutile to brookite to anatase. At first glance, this may seem counterintuitive to the purely geometric result of reconfiguring a framework with more shared edges but in fact the volume increase is a direct result of the polyhedral distortion. The reason for the volume increase can be seen in Fig. 3, where the upper two curves show that the framework Ti-Ti distances across shared edges and corners both increase due to the electrostatic repulsion from rutile to brookite to anatase, thereby increasing the volume of the crystal. With increasing shared edges, the rate of change in the average Ti-Ti distance across shared edges decreases from left to right in Fig. 3 and appears to reach a limiting value of about 3.04 Å for anatase. Conversely, the rate of change in the average Ti-Ti separation associated with the corner sharing increases and accounts for most of the volume expansion from brookite to anatase. This effect is accommodated by the increased Ti-O-Ti angles across the shared corners, which change from 130.5° in rutile to an average of 139.0° in brookite to 155.4° in anatase.

Interestingly, the octahedral volume decreases with increasing distortion. It is easy to show that, in the absence of significant changes in mean bond length, the distortion causes a decrease in volume of the coordination polyhedron. This effect is illustrated in Table I where we compare the actual octahedral volume with the volume of a perfect octahedron (θ=90°) having the same mean bond length. Another potentially useful parameter is the packing index (PI), defined as the total volume of the ions divided by the unit cell volume. The PI values in Table I demonstrate that the amount of open space in the crystalline structure follows the order rutile < brookite < anatase. This may have important implications with regard to the energetics of the defect formation in these polymorphs. As a first approximation, we might expect the defect formation energies to follow the opposite trend with the more open structure of anatase having the lowest defect energies.

The process of amorphization usually involves a substantial increase in the total volume with typical values of 5%–10% for oxides (e.g., fluorite derivatives and perovskite). Hence, the molar volume of the amorphous form of a given compound will be higher than that of the corresponding crystalline form. This is consistent with the MD simulations of fully dense TiO_2 glass conducted by Hoang,[31] who reported

a density of 3.80 g cm^{-3} from which we obtain a molar volume of 21.03 cm^3 mol^{-1}. Provided that the amorphous structures of all three polymorphs produced by ion irradiation have densities similar to that obtained in the MD simulation, the molar volume data listed in Table I suggest that the difference in volume due to the crystalline–amorphous transformation (ΔV_{ca}) is approximately 11.8 % for rutile, 8.7 % for brookite, and 2.5 % for anatase. Thus, in the absence of other effects, the component of volume strain due to the amorphous domains may contribute to the driving force for the recovery defects and may provide at least a partial explanation for the radiation response observed in this study. Note that it is also necessary to determine the strains introduced by isolated vacancies and interstitials, as these contribute to the changes in volume during irradiation.

D. Atomistic simulations

In a previous work, we calculated formation energies of 9–11 eV for split (the most common configuration), channel, and channel wall O Frenkel defects in rutile.[38] Oxygen interstitials migrate from split interstitial to split interstitial via channel sites, enabling motion in three dimensions, but are particularly active in the (001) plane. The migration energy is <0.1 eV, as estimated from static and dynamic calculations; thus, annealing is likely to occur well below room temperature. The Ti Frenkel defect energy was found to be approximately 18 eV and the Ti interstitials prefer the channel sites. The migration occurs from channel site to channel site along [001], and also by split interstitials and coordinated movements of many Ti atoms in the (001) plane, e.g., along [100]. The energy barrier for Ti migration was estimated at 0.3 eV.[38] The results presented above are generally consistent with the previous work on defect formation and migration energies in rutile and provide confirmation of the low temperature experimental data presented in this paper.

We have conducted additional static defect calculations, finding that the O Frenkel defect formation energies are very similar for all three polymorphs, with values of 9.0 eV for rutile, 9.6 eV for brookite, and 8.0 eV for anatase. With regard to the defect configurations, a common feature of all three polymorphs is the occurrence of the split oxygen interstitial. For Ti Frenkel defects, the results of the calculations give formation energies of 18.1 eV for rutile, 21.4 eV for brookite, and 7.3 eV for anatase. The data for brookite do not fit the expected pattern based upon the consideration of the PI values discussed above, indicating that there are additional complexities at the atomic scale yet to be elucidated. Based upon the absence of simple tunnels and the extent of bond length distortion, the intermediate radiation response of brookite may be found in the nature and energetics of the defect migration pathways and energy barriers with respect to those of rutile. The low defect formation energies calculated for anatase are consistent with the greater percentage of open space in the structure, providing more stable sites for O and especially for Ti interstitials.

To investigate the timescale on which the radiation damage in TiO_2 recrystallizes, we performed MD simulations of the evolution of the local regions of damage in rutile, brookite, and anatase. These simulations were performed as an alternative to large-scale cascade simulations such as recently reported for rutile and other compounds.[39] The justification for this methodology is provided in part by recent MD simulations of Santos *et al.*,[40] wherein the thermal spikes with energy distributions taken from BCA (Binary Collision Approximation) calculations had the same recrystallization efficacy as those of the thermal spike method used here. The results of the simulations are displayed in Fig. 4 wherein the evolution of small thermal spikes in rutile and anatase are illustrated as a function of time. Large displacements are initially present for both structures (top row), but after 1 ps (middle row) the rutile structure is showing significant recovery while extended disorder remains present in anatase. As the system evolves, rutile fully recrystallizes af-

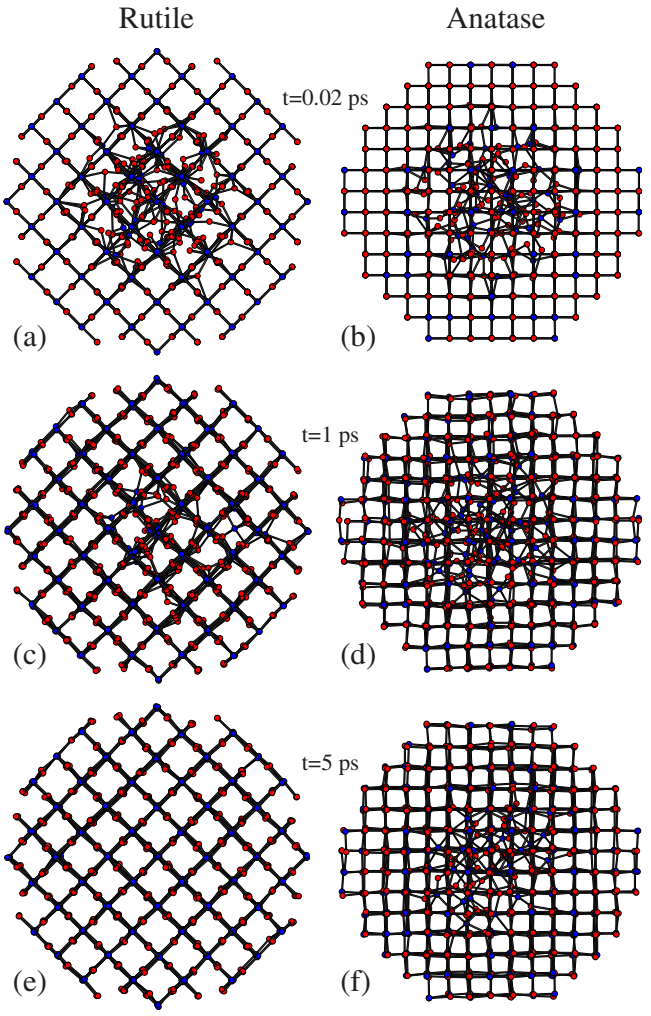

FIG. 4. (Color online) MD simulations of the evolution of small thermal spikes in rutile and anatase as a function of time: the left column is rutile and the right column is anatase. Time steps are [(a) and (b)] 0.02, [(c) and (d)] 1.0, and [(e) and (f)] 5 ps. Note the recovery of the damage volume in rutile after (e) 5 ps. In comparison, there is only a limited recovery of damage in anatase after (f) 5 ps and the amorphous pocket persists beyond this time scale. Brookite (not shown) exhibits intermediate behavior, consistent with the experimental results. Oxygen atoms are shown as white (red) spheres and titanium atoms are dark gray (blue).

ter 3 ps, while after 5 ps (bottom row), the anatase structure contains a large amorphous pocket that remains stable under the conditions of the simulation. A similar calculation (not shown) performed for brookite showed an intermediate level of damage recovery, resulting in two separated interstitial complexes comprising a total of seven atoms.

The MD simulations are in very good qualitative agreement with the experiments, showing the same relative ordering between rutile, brookite, and anatase, and demonstrating that rutile has a very strong driving force for recovery of small thermal spike damage on picosecond time scales. Considering the radius (7 Å) of the simulation sphere for atomic displacements used in the simulations, the result for rutile is in very good agreement with the calculations of Thomas *et al.*,[38] who found that the 50% probability defect recombination distance in rutile is on the order of 7–13 Å. The ease with which amorphous "pockets" are generated in anatase is consistent with the low critical fluence observed at 50 K, suggesting that the defect recombination distance is significantly smaller than that of rutile. To some extent, this may reflect the absence of low energy defect migration pathways and higher energy barriers in the distorted structure. We are currently performing a range of additional simulations to quantify the number of defects as a function of structure and time, initial spike radius, and initial kinetic energy.

V. CLOSING REMARKS

The irradiation experiments conducted at 50 K with 1.0 MeV Kr ions show that the critical fluence for amorphization is inversely correlated with the polyhedral distortion in the low-pressure TiO_2 polymorphs rutile, brookite, and anatase. We show that the polyhedral distortion in these polymorphs leads to increased molar volume through electrostatic Ti-Ti repulsion in the octahedral framework coupled with a decreased polyhedral volume. Hence, the volume of open space available increases with the distortion and provides a potential mechanism for lower defect formation energies at the preferred interstitial sites. The static defect calculations for anatase are consistent with this hypothesis; however, the calculated defect energies for brookite do not fit the observed trend, so other factors (e.g., defect migration pathways and energy barriers) must be invoked in order to explain the intermediate behavior of this polymorph.

The MD simulations of small thermal spikes do show qualitative agreement with the experiments. This is encouraging, as the computational approach may be applicable to a range of insulating oxide materials. Further studies of the defect dynamics, together with *ab initio* studies of the energetics, may shed a new light on the observed radiation response of the different polymorphs. With the information at hand, we conclude that the radiation tolerance of rutile is due in part to the presence of low energy migration pathways for both O and Ti. At the other extreme, anatase is easily amorphized at 50 K and we speculate that this behavior may be influenced by fewer low energy migration pathways and significant energy barriers to defect migration and recombination.

Previous MD simulations and experimental results on glassy and amorphous TiO_2 discussed above lead to a conceptual model for the amorphous phases produced by the irradiation of crystalline precursors. This model consists of a framework of distorted TiO_{6-x} polyhedra, with $x=0.2-0.6$, a slightly reduced mean Ti-O distance, and both edge and corner sharing between polyhedra with local configurations similar to those found in anatase and brookite.

Ultimately, the radiation tolerance of a given material will depend on the balance between defect energies, configurations, strain effects, and migration pathways and barriers.

ACKNOWLEDGMENTS

The authors thank the IVEM-Tandem Facility staff at Argonne National Laboratory for assistance during the ion irradiation work. The IVEM-Tandem Facility is supported as a User Facility by the U.S. DOE, Basic Energy Sciences, under Contract No. W-31-10-ENG-38. We acknowledge financial support from the Access to Major Research Facilities Programme (a component of the International Science Linkages Programme established under the Australian Government's innovation statement, Backing Australia's Ability). The synthetic rutile sample was provided by Lynn Boatner (Oak Ridge National Laboratory) and the natural samples of anatase and brookite were provided by Alan Pring (South Australia Museum).

APPENDIX A: CALCULATION OF DISTORTION AND VOLUME PARAMETERS

Polyhedral distortions were investigated by calculating the deviations of the Ti-O bond lengths and O-O edge lengths (d_i) from average values using the following expression:

$$\Delta = 100\sum_{i=1}^{n}[(d_i - d_{\text{ave}})/d_{\text{ave}}]^2/n. \tag{A1}$$

The bond angle variance is calculated from the individual bond angles (θ) with reference to the ideal bond angle (θ_0) for a regular polyhedron,

$$\sigma_\theta^2 = \sum_{i=1}^{n}(\theta_i - \theta_0)^2/(n-1). \tag{A2}$$

The quadratic elongation gives the degree of distortion of a polyhedron from a perfect polyhedron of the same volume, where d_0 is the bond length of the perfect polyhedron,

$$\langle\lambda\rangle = \sum_{i=1}^{n}(d_i/d_0)^2/n. \tag{A3}$$

Note that the parameters defined above are all scalar quantities and give no information about the geometry of the distortions present in the crystal. In this study, the octahedral volume was computed using the approximation given below,

$$V_{\text{oct}} = \frac{2}{3}[(d^a_{\text{O-O}})(d^b_{\text{O-O}})(d^h_{\text{Ti-O}})\sin^2\theta_h]. \tag{A4}$$

In this calculation, the octahedron is divided into two halves (along a plane of symmetry if possible). Then two O-O edge

TABLE II. Critical amorphization temperatures and fluences at low temperature determined by *in situ* TEM methods, using both crushed grains on carbon filmed copper grids and IBT sections for the same compounds.

Compound	Ref.	Method	T_c (K)	$F_c(10^{14}$ ions cm$^{-2})$	T (K)
$La_2Zr_2O_7$	42	C-Cu grid	339 ± 49	11.6 ± 2.6	50
$La_2Zr_2O_7$	43	IBT	~ 310	12.0	25
$CaZrTi_2O_7$	44	C-Cu grid	660 ± 11	3.7 ± 0.1	303
$CaZrTi_2O_7$ [a]	45	IBT	654	~ 3.9	300
$Gd2Ti_2O_7$	46	C-Cu grid	1226 ± 124	2.9 ± 0.2	300
$Gd_2Ti_2O_7$ [a]	45[a]	IBT	1110	~ 2.1	300

[a]The critical fluence is estimated from Fig. 3 in Ref. 45, as the data were not tabulated.

lengths a and b are chosen to define the area of the base of a pyramid and the Ti-O bond length h gives the distance to the apex with bond angle θ_h. This equation was also used to obtain the value of d_0 used in Eq. (A3).

APPENDIX B: COMPARISON OF EXPERIMENTAL METHODS

The use of crushed grains dispersed on carbon filmed copper grids allows the investigator to measure a selection of different grains for each experimental data point and show error bars that reflect the variations in each irradiation experiment: the important point being that the variations in thickness, orientation, and sample temperature are averaged out. Any grains that change orientation, for example, usually show up as outliers and the data are excluded. This is also true for ion channeling or adverse heating effects.

The experiments conducted with IBT samples also allow for monitoring of multiple crystals in the polycrystalline samples but not in the cases where single crystals are employed. The IBT method may also introduce an amorphous layer on the specimen and this may have an influence on the interpretation by electron diffraction. The presence of a preamorphized layer due to sample preparation has led some investigators to make TEM measurements via electron diffraction in thicker (200 nm has been suggested) parts of the wedge in order to minimize the contribution from this layer. The number of displacements per ion may be considerably higher in this case. Other complications may arise if the underlying crystalline wedge acts as a template for recrystallization of the irradiated layer.

In addition to the routine measurement of a Nd doped zirconolite reference sample, we have made a comparison of the critical fluence of crushed grains and an IBT sample of the same reference material, giving critical fluences of $4.0 \pm 0.3 \times 10^{14}$ and $3.7 \pm 0.2 \times 10^{14}$ ions cm^{-2}, respectively. For the IBT specimen, measurements were also made at two different thicknesses and we found a slight decrease in F_c for the thicker part of the specimen. Smith *et al.*[41] conducted a similar test with a different sample of Nd doped zirconolite 4M, reporting values of 3.7 ± 0.3 and $3.5 \pm 0.3 \times 10^{14}$ ions cm^{-2} for the crushed grains and ion beam thinned section, respectively. Both of these comparisons were conducted on the HVEM-Tandem instrument using 1.5 MeV Kr ions at room temperature.

The experimental fluence-temperature data exist for both methods and give nearly identical results for the fluorite related superstructures $La_2Zr_2O_7$, $Gd_2Ti_2O_7$, and $CaZrTi_2O_7$ (Table II). All experiments were performed using 1.0 MeV Kr ions except for the study of $CaZrTi_2O_7$ using crushed grains method, which was performed using 1.5 MeV Kr ions. Importantly, the critical temperatures obtained by the crushed grain method tend to be higher than those obtained using IBT samples, although they are all within the errors reported in the studies using crushed grains. Note that this is not the behavior to be expected if the grains are heating up significantly in the ion beam. Of particular relevance to this paper, the comparison given in Table II also shows that the critical amorphization fluences for each compound are generally within error at room temperature or lower.

APPENDIX C: HEAT FLOW PROBLEM

The time scale required for the dissipation of heat may be estimated for both experimental methods by using a derivation of the heat flow equation. The crushed grains are on the micrometer size scale and will dissipate heat very efficiently by radiative loss mainly to vacuum in the *in situ* TEM experiment. As a rule of thumb, the time required to dissipate heat can be estimated according to $t = h^2/k$, where h is the length scale and k is the thermal diffusivity. Assuming a value of 10^{-6} m s^{-1} for k and 10^{-7}–10^{-8} m for h (=1/2 $\times$ sample thickness), the crushed grains dissipate heat on a time scale of about 10^{-8}–10^{-9} s. This is unlikely to be greatly influenced by the much thinner underlying carbon film.

Only the central part of the IBT sample disk is irradiated, leaving a "cold" zone between this area and the sample holder. For thicker parts of the sample, h is approximately 5×10^{-4} m; however, SRIM simulations indicate that 1.0 MeV Kr ions penetrate to a maximum depth of about 10^{-6} m, thus the heat loss is estimated to occur on a time scale of approximately 10^{-6} s. This represents a maximum difference of 3 orders of magnitude but does not take into account the fact that the damaged (heated) zone sits atop the bulk of the undamaged crystal, thus complicating the heat flow problem. Nevertheless, since the irradiation times in these experiments are measured in minutes or hours, *we would not expect to see large differences in thermal behavior between the two methods*. These simple calculations generally support the experimental results presented in Table II.

*Corresponding author. FAX: +61 (0) 2 9543 7179. grl@ansto.gov.au

[1] M. Langlet, M. Burgos, C. Coutier, C. Jimenez, C. Morant, and M. Manso, J. Sol-Gel Sci. Technol. **22**, 139 (2001).
[2] S. V. Stefanovsky, S. V. Yudintsev, R. Gieré, and G. R. Lumpkin, in *Energy, Waste, and the Environment: A Geochemical Perspective*, edited by R. Gieré and P. Stille (Geological Society, London, 2004), Vol. 236, p. 36.
[3] A. El Goresy, M. Chen, L. Dubrovinsky, P. Gillet, and G. Graup, Science **293**, 1467 (2001).
[4] T. Arlt, M. Bermejo, M. A. Blanco, L. Gerward, J. Z. Jiang, J. S. Olsen, and J. M. Recio, Phys. Rev. B **61**, 14414 (2000).
[5] N. A. Dubrovinskaia, L. S. Dubrovinsky, R. Ahuja, V. B. Prokopenko, V. Dmitriev, H.-P. Weber, J. M. Osorio-Guillen, and B. Johansson, Phys. Rev. Lett. **87**, 275501 (2001).
[6] M.-Y. Kuo, C.-L. Chen, C.-Y. Hua, H.-C. Yang, and P. Shen, J. Phys. Chem. B **109**, 8693 (2005).
[7] R. Fromknecht and O. Meyer, Mater. Chem. Phys. **45**, 50 (1996).
[8] O. Meyer, I. Khubeis, R. Fromknecht, and S. Massing, Nucl. Instrum. Methods Phys. Res. B **127-128**, 624 (1997).
[9] I. Khubeis, R. Fromknecht, and O. Meyer, Phys. Rev. B **55**, 136 (1997).
[10] I. Khubeis, R. Fromknecht, S. Massing, and O. Meyer, Nucl. Instrum. Methods Phys. Res. B **141**, 332 (1998).
[11] R. Fromknecht, I. Khubeis, S. Massing, and O. Meyer, Nucl. Instrum. Methods Phys. Res. B **147**, 191 (1999).
[12] O. Meyer, I. Khubeis, and R. Fromknecht, Nucl. Instrum. Methods Phys. Res. B **148**, 752 (1999).
[13] R. Fromknecht, I. Khubeis, and O. Meyer, Nucl. Instrum. Methods Phys. Res. B **161-163**, 528 (2000).
[14] T. Hartmann, L. M. Wang, W. J. Weber, N. Yu, K. E. Sickafus, J. N. Mitchell, C. J. Wetteland, M. A. Nastasi, M. G. Hollander, N. P. Baker, C. R. Evans, J. R. Tesmer, and C. J. Maggiore, Nucl. Instrum. Methods Phys. Res. B **141**, 398 (1998).
[15] F. Li, M. Ishimaru, P. Lu, I. V. Afanasyev-Charkin, and K. E. Sickafus, Nucl. Instrum. Methods Phys. Res. B **166-167**, 314 (2000).
[16] K. E. Sickafus, J. A. Valdez, J. R. Williams, R. W. Grimes, and H. T. Hawkins, Nucl. Instrum. Methods Phys. Res. B **191**, 549 (2002).
[17] B. Jiang, J. M. Zuo, N. Jiang, M. O'Keeffe, and J. C. H. Spence, Acta Crystallogr., Sect. A: Found. Crystallogr. **59**, 341 (2003).
[18] R. Brydson, H. Sauer, W. Engel, J. M. Thomas, E. Zeitler, N. Kosugi, and H. Kuroda, J. Phys.: Condens. Matter **1**, 797 (1989).
[19] R. Brydson, H. Sauer, W. Engel, and F. Hofer, J. Phys.: Condens. Matter **4**, 3429 (1992).
[20] M. Matsui and M. Akaogi, Mol. Simul. **6**, 239 (1991).
[21] C. W. Allen, L. F. Funk, and E. A. Ryan, in *Ion-Solid Interactions for Materials Modification and Processing*, MRS Symposia Proceedings No. 396 (Materials Research Society, Pittsburgh, 1996), p. 641.
[22] J. D. Gale, J. Chem. Soc., Faraday Trans. **93**, 629 (1997).
[23] N. F. Mott and M. J. Littleton, Trans. Faraday Soc. **34**, 485 (1938).
[24] W. Smith and T. R. Forrester, J. Mol. Graphics **14**, 136 (1996).
[25] G. R. Lumpkin and R. C. Ewing, Phys. Chem. Miner. **16**, 2 (1988).
[26] G. R. Lumpkin, J. Nucl. Mater. **190**, 302 (1992).
[27] J. F. Ziegler, Nucl. Instrum. Methods Phys. Res. B **219**, 1027 (2004).
[28] G. V. Gibbs and J. V. Smith, Am. Mineral. **50**, 2023 (1965).
[29] B. Renner and G. Lehman, Z. Kristallogr. **175**, 43 (1986).
[30] K. Robinson, G. V. Gibbs, and P. H. Ribbe, Science **172**, 567 (1971).
[31] V. Van Hoang, Phys. Status Solidi B **244**, 1280 (2007).
[32] J. P. Rino and N. Studart, Phys. Rev. B **59**, 6643 (1999).
[33] G. R. Lumpkin, R. C. Ewing, B. C. Chakoumakos, R. B. Greegor, F. W. Lytle, E. M. Foltyn, F. W. Clinard, Jr., L. A. Boatner, and M. M. Abraham, J. Mater. Res. **1**, 564 (1986).
[34] V. Petkov, G. Holzhter, U. Tröge, Th. Gerber, and B. Himmel, J. Non-Cryst. Solids **231**, 17 (1998).
[35] G. Antonioli, D. Bersani, P. P. Lottici, I. Manzani, G. Gnappi, and A. Montenero, Nucl. Instrum. Methods Phys. Res. B **97**, 198 (1995).
[36] I. Manzini, G. Antonioli, D. Bersani, P. P. Lottici, G. Gnappi, and A. Montenero, J. Non-Cryst. Solids **192&193**, 519 (1995).
[37] S. O. Kucheyev, T. van Buuren, T. F. Baumann, J. H. Satcher, Jr., T. M. Willey, R. W. Meulenberg, T. E. Felter, J. F. Poco, S. A. Gammon, and L. J. Terminello, Phys. Rev. B **69**, 245102 (2004).
[38] B. S. Thomas, N. A. Marks, L. R. Corrales, and R. Devanathan, Nucl. Instrum. Methods Phys. Res. B **239**, 191 (2005).
[39] K. Trachenko, M. T. Dove, E. Artacho, I. T. Todorov, and W. Smith, Phys. Rev. B **73**, 174207 (2006).
[40] I. Santos, L. A. Marqués, and L. Pelaz, Phys. Rev. B **74**, 174115 (2006).
[41] K. L. Smith, N. J. Zaluzec, and G. R. Lumpkin, J. Nucl. Mater. **250**, 36 (1997).
[42] G. R. Lumpkin, K. R. Whittle, S. Rios, K. L. Smith, and N. J. Zaluzec, J. Phys.: Condens. Matter **16**, 8557 (2004).
[43] J. Lian, X. T. Zu, K. V. G. Kutty, J. Chen, L. M. Wang, and R. C. Ewing, Phys. Rev. B **66**, 054108 (2002).
[44] K. L. Smith, M. G. Blackford, G. R. Lumpkin, and N. J. Zaluzec, in *Scientific Basis for Nuclear Waste Management XXIII*, MRS Symposia Proceedings No. 608, edited by R. W. Smith and D. W. Shoesmith (Materials Research Society, Pittsburgh, 2000), p. 487.
[45] S. X. Wang, L. M. Wang, R. C. Ewing, G. S. Was, and G. R. Lumpkin, Nucl. Instrum. Methods Phys. Res. B **148**, 704 (1999).
[46] G. R. Lumpkin, E. J. Harvey, K. L. Smith, M. G. Blackford, and N. J. Zaluzec, Proceedings of the 15th Pacific Basin Nuclear Conference, Sydney, Australia, 2006 (unpublished), Paper No. 00228 (http://www.pacificnuclear.org/pnc/2006-Proceedings/papers.html#1).